Spatiotemporal evolution of particle puffs in transitional channel flow

Accepted to Phys. Fluids 10.1063/5.0178426

Spatio-temporal evolution of particle puffs in transitional channel flow

D. Perrone,[1] J.G.M. Kuerten,[2] L. Ridolfi,[3] and S. Scarsoglio[1]
[1)]*Department of Mechanical and Aerospace Engineering, Politecnico di Torino, 10129 Turin, Italy*
[2)]*Department of Mechanical Engineering, Eindhoven University of Technology, P.O. Box 513, 5600 MB Eindhoven, The Netherlands*
[3)]*Department of Environmental, Land and Infrastructure Engineering, Politecnico di Torino, 10129 Turin, Italy*

(*Electronic mail: davide.perrone@polito.it)

(Dated: 21 November 2023)

We study the shape evolution of puffs composed by tracers advected in a transitional channel flow. We perform a direct numerical simulation of a spatially evolving channel flow, where the inflow condition is given by a solution of the Orr-Sommerfeld equation and the flow evolves through all stages of transition up to fully developed turbulence. In this setting, we release spherical puffs of particles and track their evolution using measures derived from their approximation as ellipsoids. By varying the initial position of puffs, we characterize the spatial non-homogeneity of the flow, both with respect to the distance from the wall and, most importantly, the streamwise coordinate along which the flow evolves. Furthermore, we assess the influence of scale-dependent phenomena on puff shapes by varying the initial size of the clouds of particles. The present approach explores the interaction between flow features and advected Lagrangian structures. Additionally, it reveals the interplay between flow scales and how their balance changes during transition, where the intermittency causes large puffs to be much less elongated than smaller puffs independently of the distance from the walls.

I. INTRODUCTION

Flows experiencing transition to turbulence occur in a wide variety of settings, both natural and industrial. Due to their spatial and temporal complexity, transitional flows remain challenging to study and further efforts are needed towards their full comprehension. A laminar flow can become turbulent through a multitude of pathways. The object of this study is Klebanoff-type transition (Klebanoff, Tidstrom, and Sargent [1]), which consists of several different stages. At first, some perturbations present in the laminar base flow are linearly amplified. As they grow larger, the unstable modes begin to react between themselves, leading to nonlinear effects and amplification. Finally, transition to turbulence takes place with the full breakdown of laminar flow and the onset of the energy cascade up to the dissipative scales. While the very first stages can be analyzed through linear analysis and the study of the evolution of the eigenmodes (*i.e.* the solutions of the Orr-Sommerfeld equation), the later stages of transition bear higher complexity, due to the presence of multiple scales of motion, their mutual interactions and an overall behavior characterized by strong intermittency.

While transition is usually studied in the Eulerian perspective[2–10], the analysis of Lagrangian trajectories can prove insightful, due to the possibility of tracking the evolution of material structures in time[11,12]. The Lagrangian approach enables the possibility to explore the temporal evolution of structures and their eventual coherence, together with their relation with the carrier flow[13]. The dispersion of tracer particles in fully developed turbulent flows has been studied extensively, characterizing the Lagrangian motion of single particles[14–17], pairs[18–24], higher-order structures[25,26] and their mixing[27–30]. It is reasonable to expect that additional useful insight can be gained by the application of Lagrangian methods to the study of transitional channel flow. However, particle motion has not extensively been studied in transitional flows. Conversely, studies in transitional channel flows have dealt with heat transfer problems[31,32]. We note that the properties of a passive scalar are well approximated by tracer particles under certain conditions, namely when no feedback is exerted

Accepted to Phys. Fluids 10.1063/5.0178426

on the flow from the scalar, its timescale is smaller than the smallest dynamically relevant timescales of the carrier flow and its own molecular diffusion is smaller than turbulent diffusion[17,28].

A specific case of multiparticle structures is that of puffs, which have been studied, as of now, in homogeneous isotropic turbulence. Puffs are localized emissions of tracers, initially located in a confined region of the flow domain. As they are composed by a large number of particles, their evolution is the result of the combined action of a multitude of flow scales. Scatamacchia, Biferale, and Toschi [33] have demonstrated how the presence of pairs that separate abnormally faster or slower than the average (in their case, from the Richardson prediction) remains relevant at long times after release and is strongly correlated to the intermittency of the stretching rate and the local properties of velocity correlations. The presence of such pairs shows that flow scales larger or smaller than the average size of the puff remain relevant at any time. Bianchi *et al.* [34] have shown that, in homogeneous isotropic turbulence at a moderately high Reynolds number, particle puffs experience strong anisotropic stretching for short times (of the order of $10\tau_k$, with τ_k being the Kolmogorov time), due to the stretching mechanism of the dissipative scale, which is linked to the imbalance between the Lyapunov exponents. As puffs grow, the isotropy of the flow at the larger scales forces puffs to return spherical.

In this work, we aim to study the shape evolution of puffs released in a transitional channel flow. To do so, we perform a numerical simulation in an elongated domain bounded in one dimension. We set as inflow condition a Tollmien-Schlichting wave, obtained as solution of the spatial Orr-Sommerfeld problem. Subsequently, we release spherical sets of particles, *i.e.* the puffs, at different locations in the domain, to explore both the streamwise-dependent features of their evolution and the influence of the wall-normal distance. Given the importance of the mutual interaction between puffs and flow scales, we also release puffs of different sizes. By integrating the trajectories of all particles composing a puff, we are able to determine the evolution of its shape and its interaction with the carrier flow. The study of the Lagrangian perspective through the analysis of tracer particle trajectories has not been, as of now, extensively applied to wall-bounded transitional flows. With this work, we aim to extend previously applied methods of Lagrangian turbulent flow analysis to transitional turbulence. In this way, we characterize the interaction between multi-particle structures and transitional flow features. We also provide insight on the behavior of advected quantities in such flows, which may prove useful in the study of heat transfer and chemical dispersion.

This work is organized as follows. After this introduction, section II details the numerical simulation method, the particle tracking algorithm and the numerical tools used to track and analyze the shape of puffs. Section III shows the results obtained from our analysis. Section IV provides a discussion of our findings. Section V gives some concluding remarks. Finally, in Appendix A, some brief results on the sensitivity of our results to the number of particles contained in a puff are given.

II. METHODS

A. Direct numerical simulation

The Lagrangian trajectories employed in this work were obtained by integrating the position of tracer particles inside a numerically simulated flow field experiencing spatial transition from a laminar state to turbulence. The Navier-Stokes equations

$$\nabla \cdot \mathbf{v} = 0 \tag{1}$$

$$\frac{\partial \mathbf{v}}{\partial t} + \mathbf{v} \cdot \nabla \mathbf{v} = -\frac{1}{\rho} \nabla p + \nu \Delta \mathbf{v} \tag{2}$$

were solved in a rectangular box whose size is $L_x \times L_y \times L_z = 32\pi\delta \times 2\delta \times \pi\delta$, with x, y and z being the streamwise, wall-normal and spanwise directions, respectively, and $\delta = 1$ is the channel half-height. The no-slip boundary condition was imposed at the two walls, *i.e.* $\mathbf{v}(y = \pm 1) = 0$, while a periodic boundary condition is set along the spanwise direction. Along the streamwise direction,

only the flow field at the inlet ($x = 0$) is prescribed and the flow is let to evolve spatially up to the end of the domain. A statistically steady and spatially evolving flow is achieved by keeping constant the bulk Reynolds number $Re_b = U_b\delta/\nu = 3333$, with U_b being the bulk velocity and $\nu = 1/200$ the kinematic viscosity of the fluid. Fourier polynomials were employed to discretize the flow field along the streamwise and spanwise directions, while a Chebyshev-τ approach was used along the wall-normal direction. The number of Fourier polynomials is $N_x = 6144$ along the streamwise direction and $N_z = 192$ along the spanwise direction; $N_y = 192$ Chebyshev polynomials are used along y. By doing so, the resolution along the streamwise direction is the same as in the spectral simulations of Vreman and Kuerten [35], even with the elongated domain. The solution was advanced in time using the three-stage Runge-Kutta scheme of Spalart, Moser, and Rogers [36], using a constant time step $\Delta t^+ = 0.05$. Here and in the following, normalization by means of wall units (indicated by the $^+$ apex) is done by means of the friction velocity $u_\tau = \sqrt{\tau_w/\rho}$ and the friction length $l_\tau = \nu/u_\tau$. To compute the normalized quantities, we used the value of the wall shear stress τ_w found in the turbulent region, that is towards the end of the physical domain. Thus, the values of u_τ and l_τ used for normalization is constant everywhere. Forcing is exerted by the inflow condition, which keeps the flow rate constant in time.

In order to achieve a spatially evolving flow while employing an expansion in periodic functions along the x direction, the fringe forcing method[37], as implemented by Schlatter, Stolz, and Kleiser [38], was used. A localized forcing was applied in the final portion of the domain (from $x = 0.8L_x$ onwards, that is the fringe region); the momentum equation is modified so that the flow field at $x = 0.8L_x$ is forced back from developed turbulence to the desired inflow condition. Accordingly, the momentum equation (2) becomes

$$\frac{\partial \mathbf{v}}{\partial t} + \mathbf{v}\cdot\nabla\mathbf{v} = -\frac{1}{\rho}\nabla p + \nu\Delta\mathbf{v} + \lambda(x)(\tilde{\mathbf{v}} - \mathbf{v}), \tag{3}$$

with $\lambda(x)$ being the forcing shape function, which is nonzero only in the fringe region, while $\tilde{\mathbf{v}} = U_c(1-y^2) + A_{2D}\tilde{\mathbf{v}}'_{2D} + A_{3D}\tilde{\mathbf{v}}'_{3D}$ is the desired inflow solution and is defined as the superposition of the laminar profile and two- and three-dimensional Tollmien-Schlichting waves. The centerline velocity is U_c and the amplitudes of the perturbations are set to 6% and 0.2% of the centerline velocity (that is, $A_{2D} = 0.06U_c$ and $A_{3D} = 0.002U_c$), for two- and three-dimensional perturbations, respectively. While these values are higher than what is found in similar simulations of temporally evolving channel flow, they are chosen in order to obtain transition in a shorter length, to limit the streamwise size of the domain needed to observe the full transition to turbulence[39].

The wall-normal component of the perturbation $\tilde{v}' = \hat{v}'e^{i(\alpha x+\beta z-\omega t)}$ was obtained by solving numerically the spatially evolving Orr-Sommerfeld equation

$$\frac{\mathrm{d}^4\hat{v}}{\mathrm{d}y^4} - 2\left(\alpha^2+\beta^2\right)\frac{\mathrm{d}^2\hat{v}}{\mathrm{d}y^2} + \left(\alpha^2+\beta^2\right)^2\hat{v} - i\alpha Re_c\left(1-y^2\right)\left[\frac{\mathrm{d}^2\hat{v}}{\mathrm{d}y^2} - \left(\alpha^2+\beta^2\right)\hat{v}\right] - 2i\alpha Re_c\hat{v} = \\ = -i\omega Re_c\left[\frac{\mathrm{d}^2\hat{v}}{\mathrm{d}y^2} - \left(\alpha^2+\beta^2\right)\hat{v}\right], \tag{4}$$

where $Re_c = 3Re_b/2 = 5000$ is the centerline Reynolds number of the parabolic streamwise velocity profile, α and β are the streamwise and spanwise wavenumbers of the perturbation and $\omega = 0.3$ is the temporal wavenumber of the perturbation (which is real because the TS waves evolve only in space).

Equation 4 was solved for α, accounting both for a two-dimensional ($\beta = 0$) and a three-dimensional ($\beta = 2$) perturbation of the laminar (parabolic) profile. In the two-dimensional case, the streamwise component of the perturbation was obtained solving the continuity equation, while in the three-dimensional case Squire's equation was used

$$\frac{\mathrm{d}^2\hat{\eta}}{\mathrm{d}y^2} - \left(\alpha^2+\beta^2\right)\hat{\eta} - \mathrm{Re}_c\left[i\alpha\left(1-y^2\right) - i\omega\right]\hat{\eta} = -2i\beta y\hat{v}, \tag{5}$$

where $\hat{\eta}$ is the wall-normal component of the vorticity[40]. Equations 4-5 were solved using the same Chebyshev-τ method as the one used to discretize the flow field of the numerical simulation. The

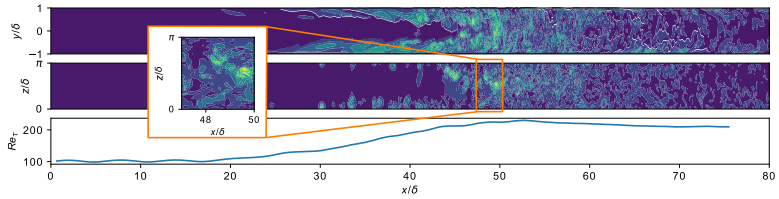

FIG. 1. In the top panels, lateral and top view of the wall-normal velocity component at a single time, with an inset detailing features of the transitional flow. In the bottom panel, frictional Reynolds number Re_τ as a function of the streamwise coordinate.

resulting nonlinear eigenvalue problem in α was solved using the companion matrix method. The eigenvalues of the spatial Orr-Sommerfeld equation are in general complex (*i.e.* the perturbation is spatially evolving). Following Schlatter, Stolz, and Kleiser[38] the least unstable eigenvalues with $Re(\alpha) > 0.5$ are chosen, thus yielding $\alpha_{2D} = 1.08 + 0.0046i$ and $\alpha_{3D} = 0.788 + 0.2106i$. In the case of a three-dimensional perturbation, Squire's equation 5, together with continuity, was used to obtain both the streamwise and the spanwise components of the perturbation.

Finally, the forcing shape function is defined as

$$\lambda(x) = \lambda_{max}\left[S\left(\frac{x-0.8L_x}{\Delta_{rise}}\right) - S\left(\frac{x-L_x}{\Delta_{fall}}+1\right)\right], \tag{6}$$

where $S(y)$ is a smooth step function defined on $\mathbb{R}$

$$S(y) = \begin{cases} 0 & \text{if } y \leqslant 0 \\ 1/\left[1+\mathrm{e}^{\left(\frac{1}{y-1}+\frac{1}{y}\right)}\right] & \text{if } 0 < y < 1 \\ 1 & \text{if } y \geqslant 1, \end{cases} \tag{7}$$

and $\Delta_{rise} = 0.12L_x$ and $\Delta_{fall} = 0.04L_x$ are shape parameters that determine how gradually the forcing is applied. Finally, λ_{max} is of the order of Δt^{-1}.

The simulation was run until all quantities are statistically stationary at all streamwise coordinates and full transition to turbulence is observed. After that, puffs of particles are released at selected locations inside the physical domain. Of course, trajectories cannot be integrated inside the fringe region because their path would not be physical. The path of each particle is integrated using the same time-stepping scheme as used for the flow simulation. The velocity at the position of particles is obtained by means of trilinear interpolation, which provides a reasonable tradeoff between accuracy and computational speed. The velocity is taken from the dealiased fields, so that the number of grid points is increased by a factor $3/2$ in the streamwise and spanwise directions[41]. In total, around $1.5 \cdot 10^9$ particles were tracked for this study.

The instantaneous wall-normal component v of the velocity field is shown in figure 1, in both a lateral view (top panel) and a top view of the flow at the center of the channel, $y/\delta = 0$ (bottom panel). The fringe region is omitted in the figure. The full transition process is clearly visible: at first only wave-like perturbations are present, which then become amplified enough to interact non-linearly, especially near the wall. The late stage of transition, taking place across the entire height of the channel, is roughly located between $x/\delta = 40$ and $x/\delta = 55$, in a region where strong velocity fluctuations are present. For $x/\delta > 55$ the flow is fully turbulent. The evolution of the flow is accompanied by an increase of wall friction, shown in figure 1 (bottom panel) through the evolution of the local friction Reynolds number $\mathrm{Re}_\tau = u_\tau \delta/\nu$. The peak of wall friction and, thus, Re_τ is located in the transitional region. The friction Reynolds number stabilizes around $\mathrm{Re}_\tau = 200$ in the turbulent region, albeit a stationary value. Finally, three mean velocity profiles taken in the laminar, transitional and turbulent regions of the flow are shown in figure 2. In the turbulent region, good agreement with the linear velocity profile for low y^+ values is found (see dotted line).

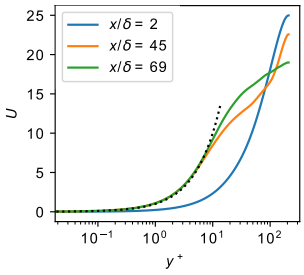

FIG. 2. Mean longitudinal velocity profiles at different streamwise locations; dotted lines: linear velocity profile at low y^+.

B. Measuring particle puff deformation

We release puffs of particles, composed of $N_p = 1024$ tracers disposed uniformly at random on a spherical surface of radius r_0. All the trajectories of particles belonging to a puff are integrated in time using the time-dependent velocity field from the channel flow simulation. Accordingly, the shape of the puff can be obtained at all times after release.

To measure the deformation of each puff, we compute the gyration tensor, that is the covariance matrix of particle positions. Following Bianchi *et al.* [34], the gyration tensor $\mathbf{G}(t)$ is defined as

$$G_{ij}(t) = \frac{1}{N_p} \sum_{n=1}^{N_p} (r_i^n(t) - \langle r_i \rangle)(r_j^n(t) - \langle r_j \rangle), \tag{8}$$

where $r_{i,n}(t)$ is the i-th component of the position of the n-th particle of the puff at time t, and $\langle r_i \rangle = \frac{1}{N_p} \sum_{n=1}^{N_p} r_{i,n}(t)$ is the coordinate of the center of mass. Some measures can be obtained from the gyration tensor and its eigenvalues λ_i, which are all non-negative. The trace of the gyration tensor (which is equal to the sum of its eigenvalues) provides the squared radius of gyration $R^2(t)$, which is a measure of the size of the puff. Notably, this measure is in very good agreement with the average distance of particles from the center of mass of the puff. The asphericity

$$A(t) = \sum_{i=1}^{3} \frac{\left(\lambda_i(t) - \overline{\lambda}(t)\right)^2}{6\overline{\lambda}^2(t)} \tag{9}$$

with $\overline{\lambda}(t)$ being the average of the three eigenvalues measures how spherical the puff is. If $A \approx 0$, all eigenvalues have similar values and the shape of the puff is spherical, while if $A = 1$ one eigenvalue dominates the others and the puff has the shape of a rod.

III. RESULTS

A. Short term deformation of puffs

In this section, we focus on the stage in which puffs are still small compared to the size of the channel δ. Because spatial non-homogeneity develops along both the x (because of the transition from laminar flow to turbulence) and y directions (because of the walls), also the properties of puffs depend on both the x and y coordinates of release. At time $t^+ = 0$ we released puffs at several locations inside the domain, covering both the streamwise evolution of the transitional flow

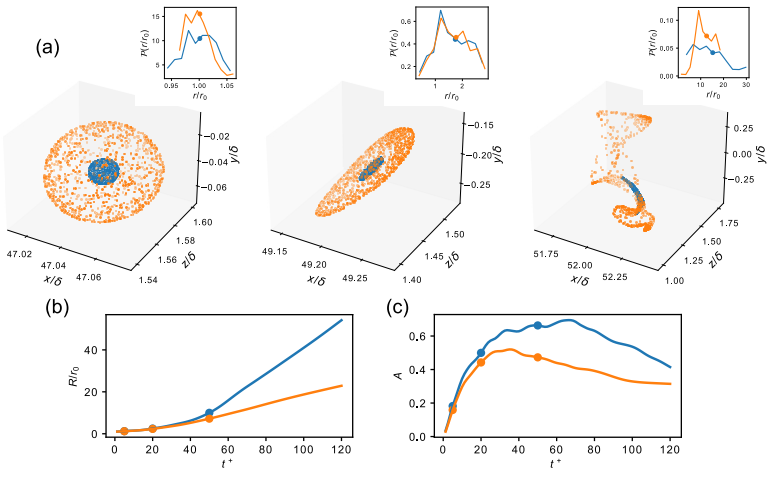

FIG. 3. a) Shape evolution of two puffs of different radii, released at the same location ($x/\delta = 46$, $y/\delta = 0$), at times $t^+ = 1.25$, $t^+ = 20$ and $t^+ = 50$; the radius of the smaller puff is $r_0^+ = 1.5$, that of the larger is $r_0^+ = 6$. In the inset, the probability density function of the distance of particles from the center of mass of the puff is shown, while dots indicate the average, *i.e.* the radius R (the distance is normalized by r_0 of the puff). b) Time evolution of the radius of the puffs shown above; dots indicate the time at which the puffs in panel a) are shown. c) Time evolution of the asphericity of puffs shown above.

and its wall-normal extension by disposing equally spaced puffs along x and y. In particular, 48 equally spaced locations were chosen along x, and 48 along y, resulting in 2304 distinct release locations covering the complete domain. For each location, we released several ($N = 128$) puffs at different times in order to obtain statistically significant results, making sure that the spacing between realizations was enough to avoid correlation issues.

The shape of a puff with initial radius $r_0^+ = 1.5$ released inside the transitional region ($x/\delta \approx 46$, $y/\delta = 0$) is shown in figure 3(a) in blue color, exemplifying the behavior of puff shape evolution. The three panels show the shape of the puff at three different times: $t^+ = 1.25$ (immediately after release), $t^+ = 20$ and $t^+ = 50$. The puff is inside the transitional region for all three times shown here, as it has traveled a distance $x/\delta \approx 5$ downstream from its release location at $t^+ = 50$. The distribution of the distance of particles from the center of mass of the puff at the same times is shown in the insets. Shortly after release, the distribution is very narrow because all particles are still close to their origin on the surface of the sphere. As time passes, the distribution widens as puffs are stretched by the flow; some particles have moved closer together, although most of them are driven further away from each other.

We observed that puffs are deformed according to the velocity field locally sampled by particles along their trajectories. Indeed, both mean shear and velocity fluctuations contribute to the modification of the shape of puffs. In the laminar region only mean shear is present (the Tollmien-Schlichting waves have no significant effect on puff shape as their behavior is cyclic) and puffs stretch along the streamwise direction. On the other hand, in the transitional and turbulent regions the complexity of the flow field reflects onto the deformation of puffs.

In order to systematically analyze the shape of puffs, we computed the quantities defined in section II. Figure 3(b)-(c) show the temporal evolution of the normalized radius of gyration, R/r_0, and the asphericity, A, for the puffs shown above (blue lines). The radius and the asphericity of puffs rapidly grow after release, following the stretching mechanism identified by Bianchi *et al.* [34], which is linked to the smallest scales of the flow. Subsequently, we observe that the asphericity decreases,

while the rate of increase of the radius grows, but the radius remains small compared to δ. Indeed, as particles sample a larger region of the domain, they are dispersed along all directions by the velocity fluctuations at larger scales, which cause a return to isotropy and are also more effective in dispersing them (leading to faster radius growth).

The cause of the end of the upward transient of the asphericity is to be found in the increase of spatial scale of the puff and its relation with the flow scales. In turn, the scale reached by puffs depends on their initial scale (at least for short times), that determines the point at which puffs are large enough to experience a decrease of the asphericity. To assess the influence of the initial size r_0 and, consequently, the scale-dependent behavior of puffs at later times, for each release point in the channel, we placed concentric puffs with different radii r_0, ranging from $r_0^+ = 0.375$ to $r_0^+ = 6$ (the set of concentric puffs closest to the wall is placed with its center at $y^+ = 6$). Figure 3 shows, in orange color, the shape and properties of a puff released at the same location as the aforementioned one, but with a radius $r_0^+ = 6$. We observe how the shapes of the two puffs evolve differently after a short time, of the order of tens of viscous units. After t^+ is around 30, the normalized radius R/r_0 of the smaller puff grows faster than that of the larger one. Similarly, the asphericity of the smaller puff is larger.

To further elucidate the role of r_0, we show in Figure 4(a) the ratio $A|_{r_0^+=1.5}/A|_{r_0^+=6}$ between the asphericity of the puffs with $r_0^+ = 1.5$ and the puffs with $r_0^+ = 6$. To do so, we released sets of concentric puffs with different values of r_0 on a grid along x and y; the ratio between the two values of the asphericity is shown here at time $t^+ = 50$. The imbalance between the asphericity of large and small puffs, already highlighted for the two puffs of figure 3(c), is present in the transitional and turbulent regions, while the asphericity of puffs of different sizes in the laminar region always have the same values (resulting in a ratio equal or very close to one).

Interestingly, the ratio between the asphericity of small and large puffs is larger in the transitional region than in the turbulent region. Figures 4(b)-(c) show the normalized radius and the asphericity with respect to the radius r_0 at three different times (the same as in Figure 3), for puffs located in the transitional region ($x/\delta = 46$) and at a wall-normal coordinate $y/\delta = 0$ (the center of the channel). While the initial evolution of puffs is independent of r_0, the imbalance arises after approximately $t^+ = 10$. Figure 4(d) also highlights how the imbalance of the asphericity is stronger in the transitional region (solid lines) with respect to the turbulent region (dotted lines). We also note how at a later time (shown in red in the figure), the asphericity of the puffs released in the transitional region is decreasing (especially that of the larger puffs), while the asphericity of puffs in the turbulent region is still increasing. While all puffs follow the general trend shown in figure 3(c), the exact time at which the asphericity starts to decrease depends on the release location of puffs. Because of this, different behaviors can be found at the same time. In both the transitional and the turbulent region, the imbalance is increasing with time.

Finally, we note that the imbalance is mostly independent of the wall-normal coordinate, as is visible from figure 4(a). The effect of shear appears to be the same on puffs of different sizes. Accordingly, the asphericity is scale-independent in the laminar region (where only mean shear is present), while its scale dependence does not depend on y in the transitional and turbulent regions.

In general, the evolution of puff shapes in the transitional and turbulent regions seems to be characterized by two distinct regimes. Both regimes take place when puffs are still smaller than the integral scale of the flow δ, but have significantly different associated behaviors. The first is tightly linked with the initial velocities of particles, due to the very short timescales involved which are well within the ballistic regime. The imbalance regime instead is scale-dependent and linked to the Lagrangian evolution of trajectories beyond the ballistic regime. The exact threshold between these two regimes, which marks the shift from growing asphericity to more spherical puff shapes, depends on the release position of puffs; nonetheless, it is present everywhere in the transitional and turbulent regions. In the following we will analyze both regimes.

1. *Ballistic regime*

The initial dispersion of particle pertains to the ballistic regime, in which only their initial velocity plays a role in determining their displacement. Indeed, particle velocities remain strongly correlated

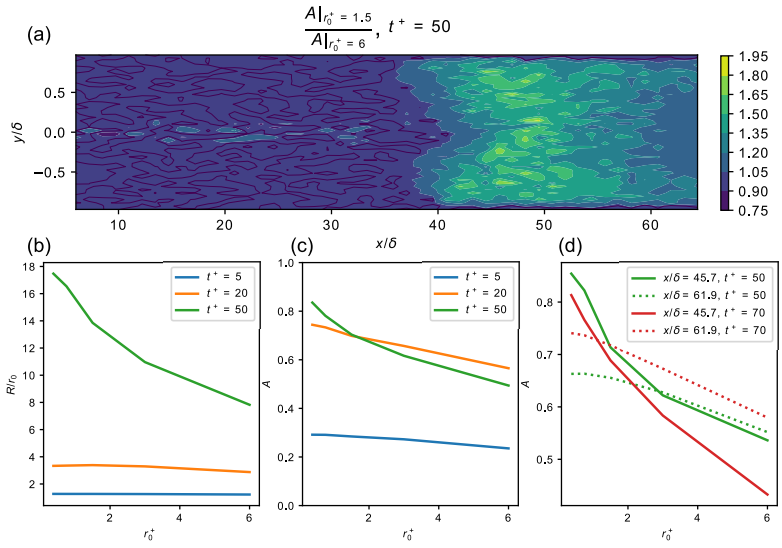

FIG. 4. a) Ratio between the asphericity for puffs with $r_0^+ = 1.5$ and puffs with $r_0^+ = 6$ at $t^+ = 50$; black contour lines indicate a ratio of one. b) Radius of puffs (normalized by the radius at release) as a function of r_0, shown at subsequent times (puffs released at $x/\delta \approx 46$, $y/\delta = 0$). c) Asphericity of puffs as a function of r_0, shown at subsequent times, same puffs as in (b). d) Asphericity of puffs shown at two different x locations ($x/\delta \approx 46$ in the transitional region and $x/\delta \approx 62$ in the region where turbulence is fully developed), $y/\delta = 0$, and at two different times.

to that at the time of release when the time is much smaller than the Lagrangian timescale. In this regime, the relative motion of particles is governed by the initial velocity differences, *i.e.* the local Eulerian structure functions

$$D_{i,j}(r) = \langle (v_i(\mathbf{x} + r\hat{\mathbf{e}}_j) - v_i(\mathbf{x}))^2 \rangle. \tag{10}$$

Although the deformation of a puff is the result of the relative motion of several ($\mathcal{O}(N_p^2)$) particle pairs, whose initial separation may be smaller than or equal to $2r_0$ (that is, the diameter of the puff), the initial stretching and straining of a puff can be related to the velocity differences at the scale of the puff.

We computed the Eulerian velocity structure function everywhere in the channel domain and at scales r up to the initial size of the largest puffs (that is, twice the value $r_{0,\max}^+ = 6$). To investigate whether the effect of the initial velocities is responsible for the appearance of the imbalance, we computed the asphericity of puffs of different sizes r_0 deformed by the effects of velocity differences at the scale of the puff. To do so, we stretched and sheared puffs using the values of the structure functions computed inside the channel flow. The coordinates of the synthetically deformed puffs were computed as

$$x_i(t) = x_i^0 + \sum_{i=1}^{3} x_j^0 \frac{t\sqrt{D_{i,j}(r_0)}}{2r_0}. \tag{11}$$

The asphericity of these puffs was found to be independent of r_0 for values of t consistent with the typical times in which no differences between the asphericity of puffs appeared, which is of the order of $t^+ = 10$ inside the transitional region (see figures 3(b)-(c)). Therefore, the effect of

the initial velocity differences is consistent with the observed initial behavior of puffs, whose shape evolves for very short times independently of r_0. Accordingly, the cause of the appearance of the shape imbalance is not to be found in initial velocity differences, but rather in their later behavior.

2. *Imbalance regime*

After the ballistic regime, puff behavior is no longer determined by the initial velocity of particles, but rather by the entire velocity field (and the corresponding flow scales) sampled by particles along their path. We observed (recall figure 4) that especially in the transitional region of the domain, but also in the turbulent region to a lesser extent, puffs with larger release size r_0 exhibit smaller asphericity than their smaller counterparts. This phenomenon is tightly linked to the second phase of the shape evolution of puffs, *i.e.* when particles are spread along three dimensions by the velocity fluctuations at intermediate scales.

We recall that puffs, after being released in the flow, are stretched into elongated shapes with high asphericity, as is shown in figure 3. After that, the dispersion of particles by velocity fluctuations at scales larger than that at release results in a decrease of the asphericity. The shift from one behavior (of growing asphericity) to another (leading to more spherical puffs) is linked to the different features of flow scales at different sizes and, accordingly, strongly depends on the scale of the puff[34]. Puffs with larger r_0 are the first to encounter the flow scales that cause the return to isotropic shapes, due to their larger initial size. Accordingly, their asphericity does not grow as large as that of smaller puffs, leading to the rise of the imbalance. Notice that, although the smaller puffs grow faster than the larger ones, as shown in figure 4(b), the non-normalized radius R of the puffs with lower r_0 always remains smaller than that of larger puffs.

In the laminar region, no imbalance appears, *i.e.* the shape of puffs with different r_0 evolves similarly at all times. Moreover, in the transitional and turbulent region the imbalance is present with similar intensity at all y coordinates. These features highlight that the y-dependent mean shear does not contribute to the appearance of the imbalance.

The ratio between the asphericity of small and large puffs is maximum in the transitional region. In figures 5(a)-(b) we show the mean and standard deviation of the three components of the acceleration of particles with respect to the wall-normal coordinate y at two streamwise locations; one is located well inside the transitional region (dotted lines), while the other is in fully developed turbulence (solid lines). Both the mean and the standard deviation of particle acceleration for puffs inside the transitional region are larger. The mean acceleration is stronger near the walls, where the flow is far from isotropy. Particles located in the transitional region are subject to intense accelerations, caused by the stronger velocity fluctuations, leading to larger puff deformations.

Additionally, we show the Lagrangian structure function

$$D_{L,i}(\tau) = \langle (v_i(t+\tau) - v_i(t))^2 \rangle, \tag{12}$$

computed starting from the velocity of particles, at the same two locations as the previous panels, in figure 5(c). Again, Lagrangian velocity differences have far larger magnitude in the transitional region, as a direct result of the more intense velocity fluctuations.

The peculiar features of the transitional region and of the particle trajectories within this region are the causes of the increased shape imbalance that we observed. Transition-induced intermittency, especially at the smaller scales of the flow, results in stronger scale-dependence of puff properties in the transitional region. Other than the single-particle statistics shown in figure 5, we have measured the acceleration of particles belonging to each puff, noticing a larger difference between the acceleration variance of small and large puffs in the transitional region than elsewhere.

In short, three main aspects of the shape evolution of puffs have emerged. First, the asphericity has a non-monotonic trend, owing to the interplay between small scales that stretch puffs and larger scales that make their shape spherical again. Furthermore, the balance between these two actions is governed by the initial size of the puff. It follows that the shape of puffs of different initial sizes evolves differently, giving rise to a shape imbalance which is tightly linked to the presence of multiple flow scales. Finally, the imbalance is maximum in the transitional region, due to the intermittency at small flow scales and the larger intensity of velocity fluctuations.

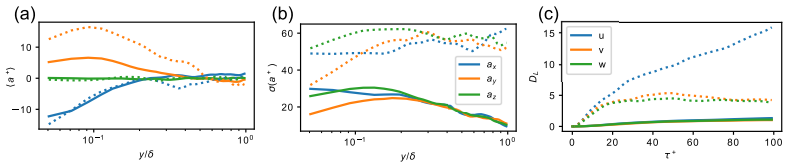

FIG. 5. (a) Mean of the acceleration of particles depending on the y coordinate. Puffs were released at $x/\delta = 47$ (dashed lines) and $x/\delta = 70$ (solid lines); (b) Standard deviation of the acceleration of particles depending on the y coordinate (same locations as panel (a)); (c) Lagrangian structure functions at the same locations of panel (a), with blue, yellow and green indicating the streamwise, wall-normal and spanwise velocity components, respectively

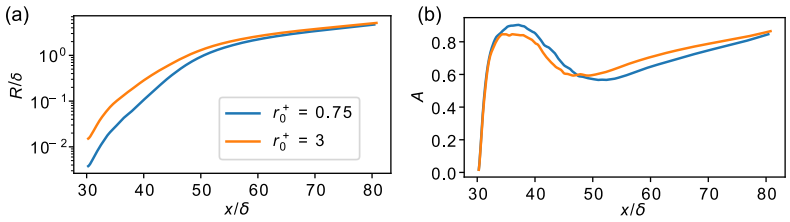

FIG. 6. (a) Radius of puffs released at $x/\delta = 30$, $y/\delta = -0.5$, with two different values of r_0; (b) Asphericity of the puffs shown in panel (a)

B. Long term behavior

While the action of isotropic flow scales causes the reduction of the asphericity observed previously, as puffs grow larger and larger they start to undergo the action of the largest, integral scales of the flow which are anisotropic because of the geometry of the domain. This is different from what was observed by Bianchi *et al.* [34] in a homogeneous and isotropic setting, where the long term behavior was that of a return to spherical puff shapes.

Figures 6(a) and (b) show the radius and the asphericity of puffs with respect to their streamwise x position. Puffs were released at $x/\delta = 30$ (just before the transitional region in the channel domain) and $y/\delta = -0.5$; two different values of r_0 are shown. The growth of R (figure 6(a)) becomes slower as puffs become larger and larger. Particles dispersion has entered Taylor's dispersion regime, when the time passed since release is much larger than the Lagrangian timescale (*i.e.* the integral up to infinity of the Lagrangian velocity autocorrelation). When the radius of puffs becomes comparable with the size of the channel δ, the main action exerted on puffs is that of the mean velocity profile, which advects particles at different velocities and thus displaces them into an elongated shape. Furthermore, the channel flow is bounded in the y direction. Both these effects contribute to the final increase of the asphericity after a local minimum is reached. As was the case for the maximum of the asphericity, the minimum is the outcome of the competing actions of the intermediate, isotropic scales and of the largest scales present in the channel that are anisotropic. For long times, differently from the imbalanced behavior previously observed, all memory regarding the initial condition (including the initial size of the puff r_0) is lost. Therefore, puffs that have been advected for a long time, such as those shown in figure 6, have similar values of the radius R and of the asphericity A independently of r_0.

IV. DISCUSSION

Results shown in the previous section show that the overall behavior of puffs depends on their release location and size, and after release is mostly conditioned by their instantaneous size (which is related to the flow scales exerting a deformation on them).

When puffs located in the transitional and turbulent regions are still small compared to the size of the channel, their shape becomes elongated at first, due to the stretching action of the smallest scales of the flow; accordingly, their asphericity increases. As their size grows, puffs sample larger region of space, whose flow scales have a dispersive effect of particles which, in turn, causes puffs to return more spherical, thus reducing their asphericity.

Given the importance of puff size in its shape evolution, we analyzed the effect of the radius at release r_0 of puffs, by releasing several puffs with different sizes at the same location. We found that their shape evolves differently depending on r_0 in the transitional and turbulent regions of the flow. In particular, smaller puffs are more elongated (and, thus, they have larger asphericity A) than their larger counterparts. This is not the case in laminar flow, where the only action exerted on puffs is that of mean shear, which appears to be the same independently of scale. The imbalance between the shapes of small and large puffs does not appear immediately. The very first phase of puff evolution is governed by Eulerian velocity differences at the scale of the puff, which we have shown to have scale-independent effects. Accordingly, for times much shorter than the Lagrangian integral timescale puffs evolve mostly independently of their initial size r_0.

After the ballistic regime, the ratio between the asphericity of small and large puffs is larger than one. Puffs with larger initial size are the first to undergo the action of the intermediate flow scales that cause the return to spherical shapes. In particular, while at smaller scales puffs still evolve according to the local stretching and therefore assume elongated, highly anisotropic shapes, at larger scales particles are instead dispersed along all directions (thus reaching near isotropic shapes) by the intermediate flow scales. These two phenomena are not clearly distinct and are instead competing, as puffs can still be stretched locally while larger flow scales reduce their asphericity. Indeed, given the high number of particles and the wide distribution of their pairwise distances, a multitude of flow scales is acting on the shape evolution of the puff at any time. The balance between the two actions is ruled by the (average) size of the puff R; when the size is small, the local stretching effects prevail, otherwise the isotropic dispersion dominates. Because of this, the imbalance of the asphericity appears to be caused by the different scales sampled at the same time by puffs with different r_0.

Most importantly, we found that the imbalance of the asphericity, at any (short) time, is maximum in the transitional region. We have shown how Lagrangian velocity fluctuations and accelerations are stronger and with larger variance in the transitional region, with respect to the rest of the flow and how these fluctuations have different spatial coherence due to small-scale intermittency.

In transitional flow, we still observe an initial growth of the asphericity of puffs at all sizes r_0. We link this behavior, which is independent of the initial scale of the puff, to the action of initial velocity differences and, ultimately, to the stretching motions at the smallest flow scales. The differences with the shape imbalance found in fully developed turbulence emerge only later, when puffs grow larger. The balance between the aforementioned competing phenomena (local stretching and larger-scale dispersion) shifts in favor of dispersion only for the larger puffs, because of the less intense velocity fluctuations at small scales (still larger than those responsible for the initial stretching). Indeed, the dispersing features of the flow are less present than in fully developed turbulence due to intermittency and the incompleteness of the energy cascade. Accordingly, the imbalance between the shape of small and large puffs is strengthened.

Finally, for very long times, all memory of the initial condition is lost and puffs become very large to the point that their deformation is mostly due to the largest scales of the flow, which because of geometrical constraints and the presence of mean flow cause puffs to become elongated along the streamwise direction. As particle trajectories at this stage have been integrated over times much longer than the integral Lagrangian timescale, the initial condition is no longer relevant to the evolution of puffs; most notably, because of this puffs behave independently of r_0.

V. CONCLUSIONS

We have analyzed the evolution of puff shapes in transitional channel flow, using a simplified representation of puffs derived from their principal axes. In particular, we focused on their radius and on the asphericity, which is a measure of how much puffs are elongated (along any direction).

We have shown the complex interplay of the Eulerian flow features of transitional channel flow and of large sets of Lagrangian tracers. The resulting phenomena of puff advection and deformation have been described with simplified measures of the shape of particle clouds. While further works may explore more complex measures and their capability to characterize the shape of puffs, we found that the measures explored in this work provide strong insight despite their straightforwardness.

The Lagrangian approach allowed us to explore some geometrical features of coherent flow structures advected by a transitional flow with strong spatio-temporal complexity. Through the analysis of puffs, we examined the interplay between flow scales of different sizes and their features. We showed how the smallest scales contribute to the stretching of puffs, while larger flow features have a more even dispersing effect on particles. Most importantly, we were able to quantify how these effects balance out depending on time and spatial position of release, by means of a multiscale analysis obtained by varying the initial size of the puffs. We found out that the imbalance between particle shape evolution is the largest in the transitional region, a finding we attribute to small-scale intermittency and the incompleteness of the inertial cascade.

Based on present findings, we have shown the validity of the study of large multiparticle structures, even in cases with a spatial complexity due to the presence of both solid boundaries and a direction along which the flow transitions to turbulence. The Lagrangian approach appears suitable to represent the complex interplay of scales that leads a perturbed laminar flow to turbulence. In particular, the study of complex multiparticle structures through simplified criteria leads to a complete description of transition even using a very reduced-order representation of puff shapes.

ACKNOWLEDGMENTS

This work was sponsored by NWO Exacte en Natuurwetenschappen (Physical Sciences) for the use of supercomputer facilities, with financial support from the Netherlands Organization for Scientific Research, NWO.

Appendix A: Sensitivity to the number of particles

The measures introduced in section II were derived from the covariance matrix of particle position which, up to statistical accuracy, is not influenced by the number of particles. Because of this, the method employed in this work is affected only slightly by the number of particles present in each puff. In figure 7, we show the same results as in figure 4(b)-(c), with the addition of data computed with puffs composed of $N_p = 625$ particles (dotted lines); the results obtained in this way are very similar to those with $N_p = 1024$. Most notably, the already discussed trends and the presence of the imbalance are unchanged. As long as particles are distributed uniformly in the puff at the time of release, no significant difference in the shape evolution emerges. Of course, the larger N_p, the more accurate the tracking of the puff shape at long times.

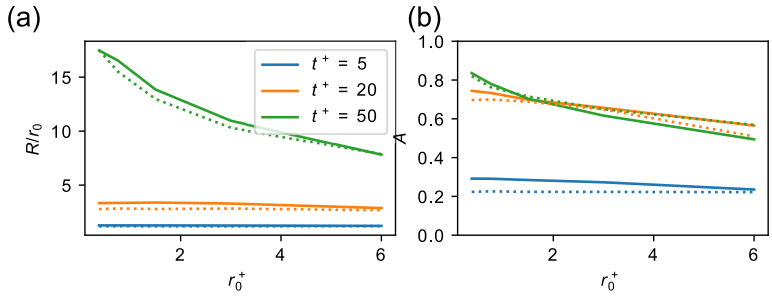

FIG. 7. a) Radius of puffs (normalized by the radius at release) as a function of r_0, shown at subsequent times (puffs released at $x/\delta \approx 46$, $y/\delta = 0$); here and in the panel on the right, the dotted lines indicate the same results computed with 625 particles, while the solid lines report the results with $N_p = 1024$. b) Asphericity of puffs as a function of r_0, shown at subsequent times (same puffs as in (a)).

[1]P. S. Klebanoff, K. D. Tidstrom, and L. M. Sargent, "The three-dimensional nature of boundary-layer instability," Journal of Fluid Mechanics **12**, 1–34 (1962).
[2]L. Kleiser and T. A. Zang, "Numerical simulation of transition in wall-bounded shear flows," Annual Review of Fluid Mechanics **23**, 495–537 (1991).
[3]N. D. Sandham and L. Kleiser, "The late stages of transition to turbulence in channel flow," Journal of Fluid Mechanics **245**, 319–348 (1992).
[4]B. Hof, J. Westerweel, T. M. Schneider, and B. Eckhardt, "Finite lifetime of turbulence in shear flows," Nature **443**, 59–62 (2006).
[5]P. Manneville, "On the transition to turbulence of wall-bounded flows in general, and plane couette flow in particular," European Journal of Mechanics - B/Fluids **49**, 345–362 (2015).
[6]M. Sano and K. Tamai, "A universal transition to turbulence in channel flow," Nature Physics **12**, 249–253 (2016).
[7]S. Gomé, L. S. Tuckerman, and D. Barkley, "Statistical transition to turbulence in plane channel flow," Phys. Rev. Fluids **5**, 083905 (2020).
[8]D. Perrone, L. Ridolfi, and S. Scarsoglio, "Visibility analysis of boundary layer transition," Physics of Fluids **34** (2022), 10.1063/5.0106455, 104104, https://pubs.aip.org/aip/pof/article-pdf/doi/10.1063/5.0106455/16580916/104104_1_online.pdf.
[9]C. Lee and X. Jiang, "Flow structures in transitional and turbulent boundary layers," Physics of Fluids **31**, 111301 (2019).
[10]M. Shimizu and P. Manneville, "Bifurcations to turbulence in transitional channel flow," Phys. Rev. Fluids **4**, 113903 (2019).
[11]Y. Zhao, Y. Yang, and S. Chen, "Evolution of material surfaces in the temporal transition in channel flow," Journal of Fluid Mechanics **793**, 840876 (2016).
[12]S. Yimprasert, M. Kvick, P. H. Alfredsson, and M. Matsubara, "Flow visualization and skin friction determination in transitional channel flow," Experiments in Fluids **62**, 1–16 (2021).
[13]F. Toschi and E. Bodenschatz, "Lagrangian Properties of Particles in Turbulence," Annual Review of Fluid Mechanics **41**, 375–404 (2009).
[14]P. K. Yeung and S. B. Pope, "Lagrangian statistics from direct numerical simulations of isotropic turbulence," Journal of Fluid Mechanics **207**, 531–586 (1989).
[15]F. Toschi, L. Biferale, G. Boffetta, A. Celani, B. J. Devenish, and A. Lanotte, "Acceleration and vortex filaments in turbulence," Journal of Turbulence **6**, N15 (2005).
[16]H. Xu, M. Bourgoin, N. T. Ouellette, and E. Bodenschatz, "High Order Lagrangian Velocity Statistics in Turbulence," Physical Review Letters **96**, 024503 (2006).
[17]N. Stelzenmuller, J. I. Polanco, L. Vignal, I. Vinkovic, and N. Mordant, "Lagrangian acceleration statistics in a turbulent channel flow," Physical Review Fluids **2**, 054602 (2017).
[18]L. Biferale, G. Boffetta, A. Celani, B. J. Devenish, A. Lanotte, and F. Toschi, "Lagrangian statistics of particle pairs in homogeneous isotropic turbulence," Physics of Fluids **17** (2005), 10.1063/1.2130742, 115101, https://pubs.aip.org/aip/pof/article-pdf/doi/10.1063/1.2130742/15709332/115101_1_online.pdf.
[19]J. P. Salazar and L. R. Collins, "Two-Particle Dispersion in Isotropic Turbulent Flows," Annual Review of Fluid Mechanics **41**, 405–432 (2009).
[20]J. Jucha, H. Xu, A. Pumir, and E. Bodenschatz, "Time-reversal-symmetry breaking in turbulence," Phys. Rev. Lett. **113**, 054501 (2014).
[21]L. Biferale, A. S. Lanotte, R. Scatamacchia, and F. Toschi, "Intermittency in the relative separations of tracers and of heavy particles in turbulent flows," Journal of Fluid Mechanics **757**, 550–572 (2014).

[22]D. Buaria, B. L. Sawford, and P. K. Yeung, "Characteristics of backward and forward two-particle relative dispersion in turbulence at different Reynolds numbers," Physics of Fluids **27**, 105101 (2015).
[23]J. I. Polanco, I. Vinkovic, N. Stelzenmuller, N. Mordant, and M. Bourgoin, "Relative dispersion of particle pairs in turbulent channel flow," International Journal of Heat and Fluid Flow **71**, 231–245 (2018).
[24]G. Elsinga, T. Ishihara, and J. Hunt, "Non-local dispersion and the reassessment of richardson's t3-scaling law," Journal of Fluid Mechanics **932**, A17 (2022).
[25]S. S. Girimaji and S. B. Pope, "Material-element deformation in isotropic turbulence," Journal of Fluid Mechanics **220**, 427–458 (1990).
[26]L. Biferale, G. Boffetta, A. Celani, B. J. Devenish, A. Lanotte, and F. Toschi, "Multiparticle dispersion in fully developed turbulence," Physics of Fluids **17**, 111701 (2005).
[27]G. Iacobello, S. Scarsoglio, J. Kuerten, and L. Ridolfi, "Lagrangian network analysis of turbulent mixing," Journal of Fluid Mechanics **865**, 546–562 (2019).
[28]D. Perrone, J. G. M. Kuerten, L. Ridolfi, and S. Scarsoglio, "Wall-induced anisotropy effects on turbulent mixing in channel flow: A network-based analysis," Phys. Rev. E **102**, 043109 (2020).
[29]D. Perrone, J. G. M. Kuerten, L. Ridolfi, and S. Scarsoglio, "Network analysis of reynolds number scaling in wall-bounded lagrangian mixing," Phys. Rev. Fluids **6**, 124501 (2021).
[30]D. Perrone, J. G. M. Kuerten, L. Ridolfi, and S. Scarsoglio, "Investigating the magnitude and temporal localization of inertial particle mixing in turbulent channel flows," International Journal of Multiphase Flow **165**, 104489 (2023).
[31]U. Ciri and S. Leonardi, "Heat transfer in a turbulent channel flow with super-hydrophobic or liquid-infused walls," Journal of Fluid Mechanics **908**, A28 (2021).
[32]W. I. Machaca Abregu, E. A. Dari, and F. E. Teruel, "Dns of heat transfer in a plane channel flow with spatial transition," International Journal of Heat and Mass Transfer **209**, 124110 (2023).
[33]R. Scatamacchia, L. Biferale, and F. Toschi, "Extreme events in the dispersions of two neighboring particles under the influence of fluid turbulence," Phys. Rev. Lett. **109**, 144501 (2012).
[34]S. Bianchi, L. Biferale, A. Celani, and M. Cencini, "On the evolution of particle-puffs in turbulence," European Journal of Mechanics - B/Fluids **55**, 324–329 (2016), vortical Structures and Wall Turbulence.
[35]A. W. Vreman and J. G. M. Kuerten, "Comparison of direct numerical simulation databases of turbulent channel flow at Re = 180," Physics of Fluids **26**, 015102 (2014), https://pubs.aip.org/aip/pof/article-pdf/doi/10.1063/1.4861064/13892632/015102_1_online.pdf.
[36]P. R. Spalart, R. D. Moser, and M. M. Rogers, "Spectral methods for the navier-stokes equations with one infinite and two periodic directions," Journal of Computational Physics **96**, 297–324 (1991).
[37]J. Nordström, N. Nordin, and D. Henningson, "The fringe region technique and the fourier method used in the direct numerical simulation of spatially evolving viscous flows," SIAM Journal on Scientific Computing **20**, 1365–1393 (1999).
[38]P. Schlatter, S. Stolz, and L. Kleiser, "Large-eddy simulation of spatial transition in plane channel flow," Journal of Turbulence **7**, N33 (2006).
[39]P. C. Schlatter, *Large-eddy simulation of transition and turbulence in wall-bounded shear flow*, Ph.D. thesis, ETH Zurich (2005).
[40]P. J. Schmid and D. S. Henningson, "Eigensolutions to the viscous problem," in *Stability and Transition in Shear Flows* (Springer New York, New York, NY, 2001) pp. 55–98.
[41]J. G. M. Kuerten and J. J. H. Brouwers, "Lagrangian statistics of turbulent channel flow at Re_τ= 950 calculated with direct numerical simulation and langevin models," Physics of fluids **25**, 105108 (2013).